JOURNAL OF PROPULSION AND POWER
Vol. 13, No. 2, March–April 1997

Spray Characteristics of Liquid Jet Traversing Subsonic Airstreams

Takao Inamura*
Hirosaki University, Hirosaki 036, Japan
and
Nobuki Nagai†
Hachinohe National College of Technology, Hachinohe 031, Japan

The spray characteristics of a liquid jet traversing subsonic airstreams were experimentally investigated. The disintegration phenomena of liquid jets were observed by instantaneous photographs and high-speed video movies. The waves on the liquid jet surface are three dimensional and show very complicated behaviors. These waves are an important cause of the liquid jet disintegration. Droplet mass fluxes were measured using an isokinetic sampling probe. Empirical equations of their distributions that are expressed by the standard normal function were deduced. Droplet sizes and droplet velocities were measured by a phase Doppler particle analyzer. At low air velocity, the mean droplet diameter reaches its maximum in the peripheral mixing region. At high air velocity, however, the mean droplet diameter reaches its maximum in the core region. The droplet velocity peaks in the peripheral mixing region over the whole range of the air velocity.

Nomenclature

A = constant in Eq. (2)
B = constant in Eq. (3)
C = constant in Eq. (5)
D = droplet size
d = inner diameter of liquid nozzle
M_a = air Mach number
m'' = droplet mass flux
m''_p = maximum droplet mass flux
m''_0 = liquid mass flux at liquid nozzle exit, $\rho_j V_j$
q = liquid-to-air momentum ratio, $\rho_j V_j^2/\rho_a V_a^2$
Re_j = liquid jet Reynolds number, $V_j d/\nu_j$
U = relative velocity between liquid and air
V_a = representative air velocity in Z direction
V_d = droplet velocity in Z direction
V_j = injection velocity of liquid jet
$W_{X1/2}$ = width of droplet mass flux profile at position where mass flux is half of maximum mass flux in X plane
$W_{Y1/2}$ = width of droplet mass flux profile at position where mass flux is half of maximum mass flux in $Y = 0$ plane
X = distance from liquid nozzle exit in direction of liquid jet injection
X_p = X at position where droplet mass flux is maximum
Y = distance from center axis of wind tunnel in the direction perpendicular to X and Z axis
Z = distance from windward liquid nozzle edge in direction of airflow
α = constant in Eq. (2)
β = constant in Eq. (2)
γ = constant in Eq. (3)
δ = constant in Eq. (3)
ε = constant in Eq. (5)
ζ = constant in Eq. (5)
ν = kinetic viscosity
ρ = density

Subscripts
a = air
d = droplet
j = liquid jet
X = in X plane
Y = in $Y = 0$ plane

Received Jan. 22, 1996; revision received Sept. 6, 1996; accepted for publication Sept. 19, 1996.
*Professor, Faculty of Science. Member AIAA.
†Director.

Introduction

THE disintegration phenomena of a liquid jet that was traversing an airstream were observed in liquid-fueled combustors, for example, in the afterburner of a jet engine or in a liquid-fueled ramjet engine. The ramjet engine has recently attracted attention as a potential space plane engine. The information about performances of the ramjet combustor has been made available on a gradual basis. In the case of the liquid-fueled ramjet engine, the atomization of a liquid fuel jet in a high-speed airstream will be considered. The liquid fuel jet disintegrates into small particles because of the shear force between a fuel jet and the airstream. It breaks up into liquid clumps farther downstream of its own accord. A liquid clump then disintegrates into finer particles. The spray characteristics of atomized fuel are very important for the design of combustors because they greatly influence combustion characteristics, for example, the evaporation rate of fuel, flame holding, combustion efficiency, etc.

Liquid jet disintegration has been investigated by some researchers in a supersonic or hypersonic airstream. Schetz and his colleagues studied liquid jet disintegration in a supersonic airstream.[1–3] They deduced empirical equations for penetration and jet width, and they measured droplet sizes and droplet mass flux distributions in a supersonic airstream.[4,5] Catton et al.[6] deduced theoretical equations for jet penetration in a hypersonic airstream. Heister et al.[7] proposed a model for the behavior of liquid jets that were injected transversely into a supersonic crossflow. Forde et al.[8] studied the penetration of liquid jets in a supersonic flow theoretically and compared them with experiments.

In a subsonic airstream, Schetz and Padhye[9] deduced the empirical equation of liquid jet penetration. They also mea-

sured droplet sizes. Kashiwagi et al.[10] studied droplet mass flux distributions of a liquid jet that was traversing a subsonic airstream. They deduced the empirical equations of mean droplet diameter and jet penetration. Recently, Oda et al.[11] have investigated liquid jet breakup in subsonic airstreams. They measured droplet mass fluxes and droplet sizes.

However, the spray characteristics of a liquid jet that was injected into a subsonic airstream are not fully understood regarding the rational design of a combustor. In particular, changes in droplet size and droplet mass flux distribution along the spray flow have not been clarified in detail in spite of their importance. Spray behavior measurements along the stream line are also required to verify the predictions by means of numerical simulation of the spray flow. They are useful in the construction of a realistic liquid breakup model.

Our series of studies aims to clarify in detail the disintegration mechanism and the spray flow of a liquid jet traversing subsonic airstreams and to contribute to the design of a liquid-fueled ramjet combustor. In a previous paper, empirical equations of jet penetrations and jet widths of a liquid and a slurry in a subsonic airstream had been deduced.[12] In this paper, the droplet mass flux distribution, mean droplet size distribution, and droplet velocity distribution were measured in detail at several downstream locations. Furthermore, empirical equations for droplet mass flux distributions were deduced.

Experimental Apparatus and Instruments

The experimental apparatus is shown in Fig. 1. The air is supplied from a blower (1) to a wind tunnel (4), passing through a settling chamber (2) and an air nozzle (3). After passing through the wind tunnel, the air-droplets two-phase flow is ejected into the ambient air and then it is exhausted by a fan (5). The blower is driven by a motor (6) whose rotational speed is controlled by an inverter (7). The air velocity is adjusted by changing the rotational speed of the motor. The liquid is supplied from a pressure vessel (8) to a liquid nozzle (11). The pressure in the vessel (8) was kept constant during experiments by a pressure regulator (9). The flow rate of the liquid is measured by an electromagnetic flow meter (10).

Figure 2 depicts details of the wind tunnel and the employed coordinate system. The wind tunnel is a subsonic blowdown type and has a rectangular cross section of 60 × 60 mm and a length of 350 mm. Two Pyrex® glass plates are attached to both sides of the wind tunnel for easy observation. Liquid nozzles with inner diameters of 1 and 2 mm and lengths of 20 and 40 mm, respectively, were used. These nozzles have a length-to-diameter ratio of 20. The liquid flow at the nozzle exit seems to be an almost fully developed turbulent flow. The details of the liquid nozzles are delineated in Fig. 3. The coordinate system is right-hand, where the X coordinate is in the direction of the liquid jet injection, the Y coordinate is in the direction of the width of the wind tunnel, and the Z coordinate is in the direction of the airflow. The origin of the coordinate system is placed at the upstream side of the liquid nozzle tip as shown in the figure.

The disintegration phenomena of a liquid jet were observed by instantaneous photographs and high-speed video movies with a frame speed of 40,000 fps.

Local droplet mass flux was measured by an isokinetic sampling probe. Figure 4 shows the sampling probe in detail. It has an i.d. of 1.2 mm and an o.d. of 3.0 mm. The isokinetic conditions in the sampling probe were maintained by adjusting the velocity and static pressure in the flow stream ahead of the probe. Two static pressure holes were provided 10 mm downstream from the probe entrance for this purpose. Local droplet mass flux was calculated from the total weight of collected droplets and the sampling time. The total weight of the collected droplets was measured by an electric balance that has high accuracy. Experimental uncertainties for the droplet sampling system are estimated to be less than 5%.

Droplet sizes and droplet velocities were measured simultaneously by a phase Doppler particle analyzer with a 10-mW He-Ne laser (PDA, Dantec Electronics Inc.). The sizing resolution of the PDA was around 1.7 μm according to the catalogue. The optical setup is summarized as follows: laser wavelength 0.6328 μm, focal length 600 mm, fringe spacing 6.33 μm, fringe number 85, waist 537 μm, maximum measurable droplet size 419 μm, and maximum measurable droplet

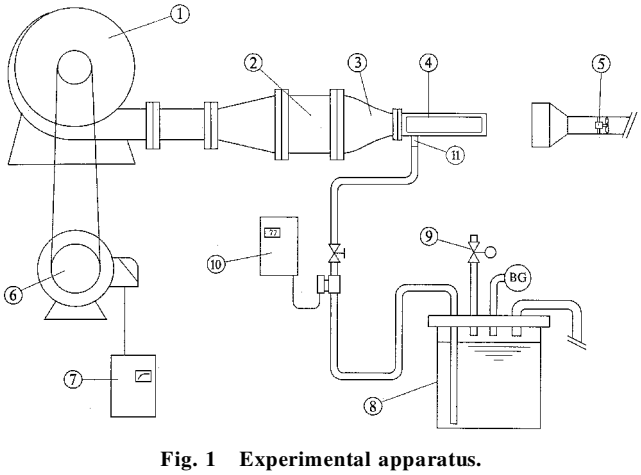

Fig. 1 Experimental apparatus.

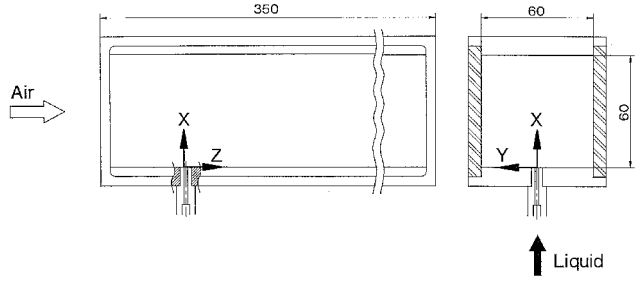

Fig. 2 Details of wind tunnel.

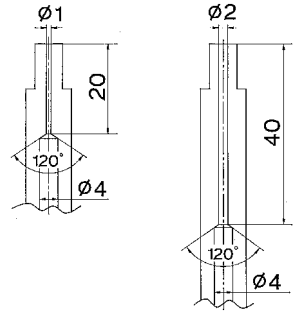

Fig. 3 Details of liquid nozzles.

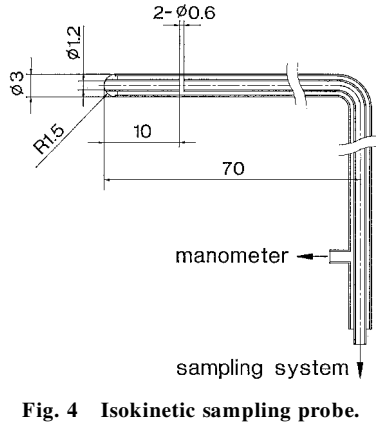

Fig. 4 Isokinetic sampling probe.

velocity 222 m/s. Averaged quantities were calculated by collecting 5000 valid sample data for each measurement point. It was estimated by Bowen and Davies[13] that to obtain 95% confidence for a measurement of droplet size, more than 5500 droplets should be measured. The repeatabilities for the measurements of mean droplet size and mean droplet velocity were more than 95%.

Experiments were carried out under the following conditions: air velocity range was from 75 to 110 m/s (M_a = 0.22 – 0.32), liquid injection velocities varied from 6.4 to 13.2 m/s (Re_j = 6.4 × 10^3 – 2.64 × 10^4), and liquid-to-air momentum ratios were limited to 6.0, 9.0, and 12.0. These conditions were determined keeping in mind the operating conditions of a ramjet engine. All experiments were carried out using tap water as the injectant.

Results and Discussion

Air Velocity Distribution

The air velocity distribution near the liquid nozzle was measured by a hot wire anemometer without liquid injection. The air velocities were almost uniform over the wind-tunnel cross section. Variations in the mean air velocity in the cross section were less than 4% of the maximum mean velocity, except in the boundary layer. Boundary-layer thickness was around 2 mm at the exit of the liquid nozzle. The turbulence component was less than 5% of the mean air velocity over the range of present experimental conditions. Representative air velocity was defined by measurement at the center of the wind tunnel just above the liquid nozzle windward edge with liquid injection.

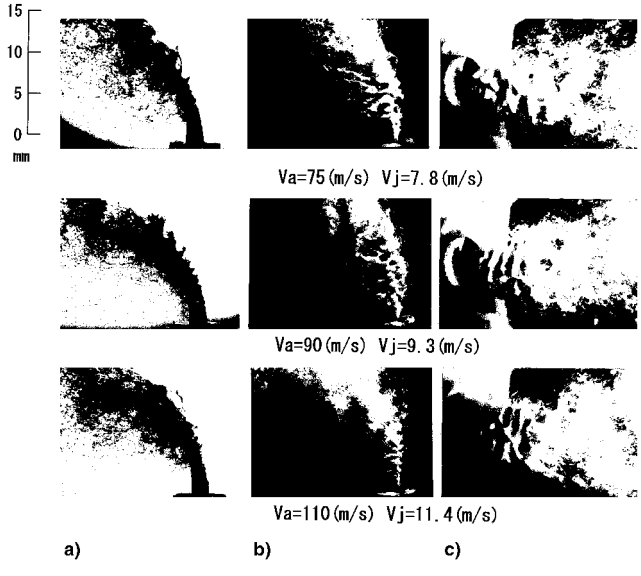

Fig. 5 Photographs of liquid jet breakup: a) side, b) right-top, and c) top views.

Disintegration Phenomena of Liquid Jet

Figure 5 shows instantaneous photographs of typical disintegration phenomena of a liquid jet from a liquid nozzle with d = 2 mm. Photographs show the evolution of disintegration processes with respect to air velocity under constant liquid-to-air momentum ratio. The liquid jet penetrates perpendicularly into a subsonic airstream near the liquid nozzle exit and is then bent downstream. From Thomas and Schetz's study,[3] the cross section of a liquid jet is almost circular near the nozzle exit and then is transformed into a kidney shape by the dynamic pressure of an airstream. This shape transformation appears to cause an increase in the drag force and the interaction with the liquid jet results in rapid downstream bending. By means of observation using magnified photographs, in the vicinity of the point where the liquid jet bends downstream rapidly, the disturbance waves on the liquid jet surface were greatly amplified.

Figure 5a shows side-view photographs. The disturbance waves on the jet windward surface look two dimensional and their wavelengths decrease with an increase in air velocity. The disturbance wave is amplified rapidly downstream along a jet surface and then it results in liquid jet disintegration. Thus, the disturbance wave on the windward surface of the liquid jet plays an important role in liquid disintegration. Figure 5b shows right-top-view photographs that were taken simultaneously with those in Fig. 5a. Figure 5c shows top-view photographs. A small amount of white paint was added in the injectant water for better visualization. It was confirmed that physical properties of the injectant scarcely changed by the addition of this paint. From Fig. 5a the surface wave looks two dimensional, however, Figs. 5b and 5c show waves that look more complex. At low air velocity, regular disturbance waves that look to be two-dimensional appear on the surface. However, at high air velocity, the regular motion of the surface wave is no longer recognizable. Numerous hollows were observed on the liquid jet surface instead.

Vertical Distribution of Droplet Mass Flux

Local droplet mass flux distributions were measured using an isokinetic sampling probe. Figure 6 shows the variation in droplet mass flux distribution in a Y = 0 plane for a 1-mm jet at several horizontal locations. The mass flux distribution peak has a vertical location that approaches the center of the wind tunnel from the exit of the liquid nozzle with an increase in momentum ratio. The maximum mass fluxes decrease downstream. The influence of the liquid-to-air momentum ratio on the maximum mass flux, however, is small.

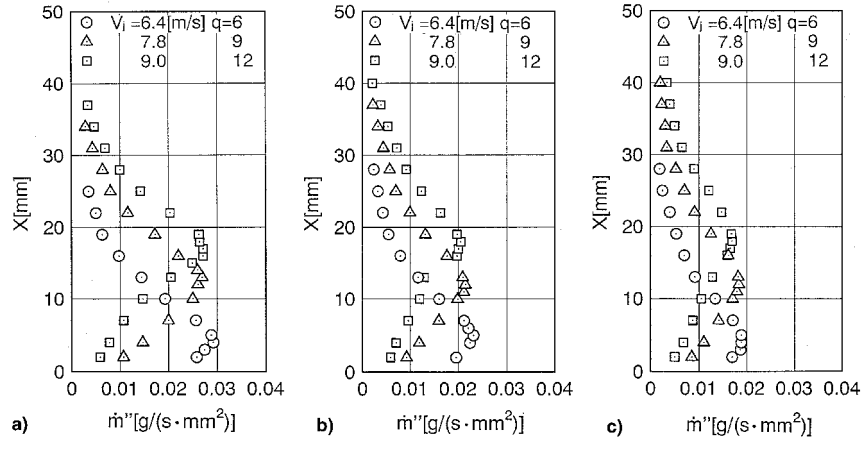

Fig. 6 Variations of droplet mass flux distribution with momentum ratio. Z = a) 100, b) 140, and c) 180 mm.

Table 1 Constants in Eq. (2) (in upper region)

d, mm	A	α	β
1.0	0.96	0.06	0.46
2.0	0.22	0.21	0.79

Table 2 Constants in Eq. (2) (in lower region)

d, mm	A	α	β
1.0	0.92	−0.17	0.60
2.0	0.56	−0.04	0.71

Table 3 Constants in Eq. (3)

d, mm	B	γ	δ
1.0	0.19	−0.31	−0.73
2.0	0.40	−0.31	−0.98

The mass flux distribution function of a two-phase flow is generally expressed by the standard normal function.[14] In this study it is assumed the empirical distribution function can be expressed by the following equation:

$$\frac{\dot{m}''_Y}{\dot{m}''_p} = \exp\left[-0.693\left(\frac{X - X_p}{W_{Y1/2}}\right)^2\right] \tag{1}$$

$W_{Y1/2}$ is a function of q and Z. Therefore, it is assumed as follows:

$$W_{Y1/2}/d = Aq^{\alpha}(Z/d)^{\beta} \tag{2}$$

The half-width in the upper region of the jet plume beyond the jet centerline is different than that in the lower region. Therefore empirical constants, A, α, and β in the previous equation were obtained separately in the upper and lower regions by the least-square method as shown in Tables 1 and 2, respectively. As shown in Tables 1 and 2, α is plus in the upper region and is minus in the lower region. This means that the droplet dispersion is increased in the upper region and is lessened in the lower region with an increase in the liquid-to-air momentum ratio.

In the case of a droplet-laden jet that was injected into still air, β equals unity.[15,16] In the present study, β is less than unity, and this appears to be because of wind tunnel walls that restrain the turbulent dispersion of spray droplets.

$\dot{m}''_p$ can be assumed similarly regarding the half-width as follows:

$$\dot{m}''_p/\dot{m}''_0 = Bq^{\gamma}(Z/d)^{\delta} \tag{3}$$

where m''_0 equals $\rho_j V_j$. The empirical constants, B, γ, and δ were obtained by the least-square method as shown in Table 3.

Hetsroni and Sokolov[15] reported that δ equals −2 for a uniform droplet-laden jet injected into still air. Yatsuyanagi,[16] however, reported that δ equals −1.5 for an airblast atomization into still air. In Hetsroni and Sokolov's study,[15] particle loading is small and the influence of particles on the airflow decays. This causes a smaller δ than that for a dense spray jet. Furthermore, in the present study, the wind-tunnel walls restrained droplet dispersion. This causes a gentle streamwise decrease in maximum droplet mass flux and results in a smaller absolute value of δ.

Figure 7 shows the variation of droplet mass flux distribution in the Z direction. The solid line indicates a comparison of experiments and calculations from Eq. (1). The distribution becomes flat downstream. The vertical location where the mass flux reaches a maximum of d = 2 mm is higher than that of

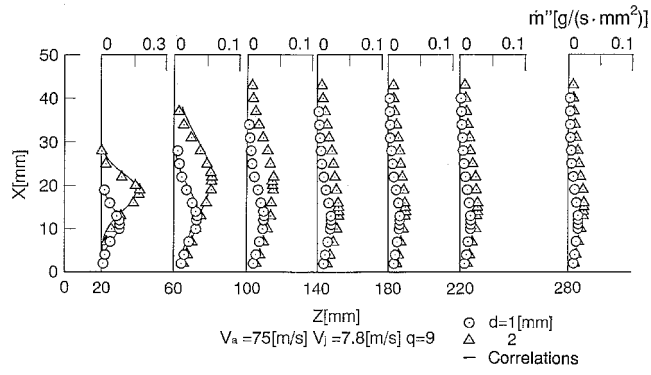

Fig. 7 Variations of droplet mass flux distribution downstream.

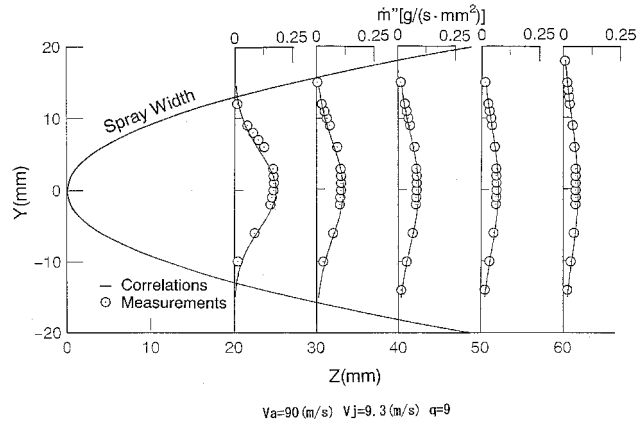

Fig. 8 Comparisons between measurements and calculations of horizontal distributions.

d = 1 mm, and the maximum mass flux of d = 2 mm is also larger than that of d = 1 mm. Since the liquid-to-air momentum ratio is kept constant, the liquid injection velocity is also kept constant. Therefore, the liquid flow rate of d = 2 mm is four times as large as that of d = 1 mm. This causes a higher X location for the peak as well as its larger mass flux of d = 2 mm.

As shown in Fig. 7, the vertical location where the mass flux reaches its maximum does not change downstream of Z = 100 mm with d = 1 mm. That of d = 2 mm, however, approaches the bottom wall downstream of Z = 100 mm because of gravity. The liquid injection nozzle of d = 2 mm generates relatively larger droplets than that of d = 1 mm. Some larger droplets lose their momentum in the X direction up to Z = 100 mm, and then fall down because of gravity. Upstream of Z = 100 mm, droplet dispersions in the X direction are almost dominated by momentum in the X direction at the time of injection. Downstream of Z = 100 mm, however, the airflow and the gravity dominate them. An empirical equation of droplet mass flux distribution was deduced in the region where the droplet dispersion is dominated by the droplet momentum, that is, $Z \leq 60$ mm.

Horizontal Distribution of Droplet Mass Flux

The mass flux distribution in a Y = 0 plane can be presented by means of the error function. Accordingly, the empirical distribution function of the droplet mass flux in the X plane was assumed to be expressed by the standard normal function as follows:

$$\dot{m}''_x/\dot{m}''_p = \exp\{-0.693(Y/W_{X1/2})^2\} \tag{4}$$

$W_{X1/2}$ is a function of q and Z, therefore, it is assumed as follows:

$$W_{X1/2}/d = Cq^{\varepsilon}(Z/d)^{\xi} \tag{5}$$

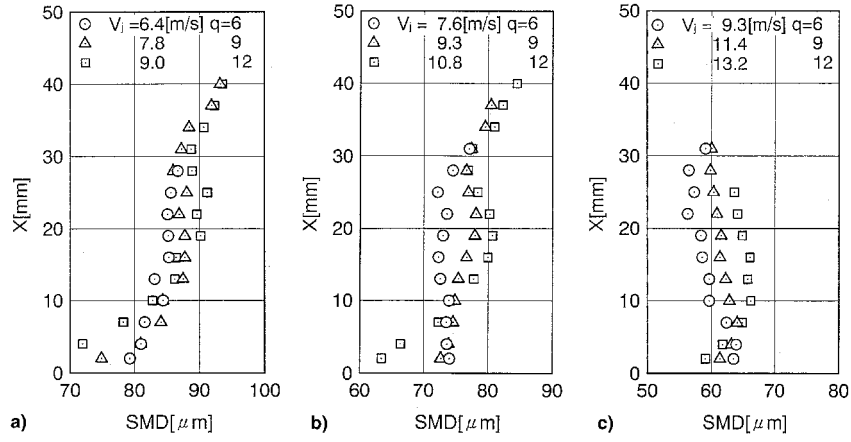

Fig. 9 Variations of mean droplet size distribution with momentum ratio. V_a = a) 75, b) 90, and c) 110 m/s.

C, ε, and ζ are empirical constants, and were 0.636, 0.195, and 0.532 for the 2-mm jet, respectively. $\dot{m}''_p$ is obtained from Eq. (3). In addition, for the horizontal distribution, ζ is less than unity as mentioned earlier. Horizontal droplet dispersion is slightly promoted with an increase in the liquid-to-air momentum ratio. As shown in our previous paper,[17] spray width is independent of the liquid nozzle diameter. Therefore, the effect of the liquid nozzle diameter on the horizontal distribution of droplet mass flux appears to be small.

Figure 8 shows droplet mass flux distribution in the X plane for a 2-mm jet at the location where droplet mass flux distribution in a $Y = 0$ plane is at its peak. The lines of spray width are calculated from an empirical equation that was deduced by Inamura et al.[17] Solid lines of droplet mass flux distribution indicate comparisons of the experiments and calculations from Eq. (4). The mass flux distribution peak becomes lower and the distribution becomes wider downstream. The distribution shows an almost symmetrical profile to the $Y = 0$ plane at every downstream location.

From comparisons between the measurements and calculations that are shown in Fig. 8, the curve-fits agree reasonably well with measurements.

Droplet Size

Droplet sizes and velocities were measured simultaneously by PDA. Figure 9 shows the variation of the mean droplet size distribution for a 1-mm jet with a liquid-to-air momentum ratio under several air velocities at $Z = 180$ mm. At low air velocity, the droplet size reaches its maximum at the periphery of a jet plume. At high air velocity, however, it reaches its maximum in the core region. At low air velocity, larger droplets penetrate the airstream and some of them can arrive at the periphery because of their larger inertia. At high air velocity, even larger droplets cannot penetrate the airstream very far because of the large aerodynamic drag force, and the periphery is occupied by the finer droplets that are detached from the jet's surface by aerodynamic shear force. From Nejad and Schetz's experiments[4] done under the supersonic airflow conditions, droplet size reaches its maximum in the core region. Oda et al.,[11] however, pointed out that droplet size achieves its maximum value at the periphery over the air velocity range less than 140 m/s.

Figure 10 shows the variation of mean droplet size distribution in the Z direction at $V_a = 75$ m/s. With $d = 1$ mm, in the vicinity of the liquid nozzle exit, Sauter mean diameter (SMD) becomes large both in the core region and in the periphery. SMD in the periphery increases downstream and eventually it reaches its maximum in the periphery farther downstream. For a 2-mm jet, in the vicinity of the nozzle exit, SMD distribution peaks in the core region. SMD in the periphery increases and in the core region it decreases. As a consequence, SMD in the periphery reaches its maximum in sections farther downstream.

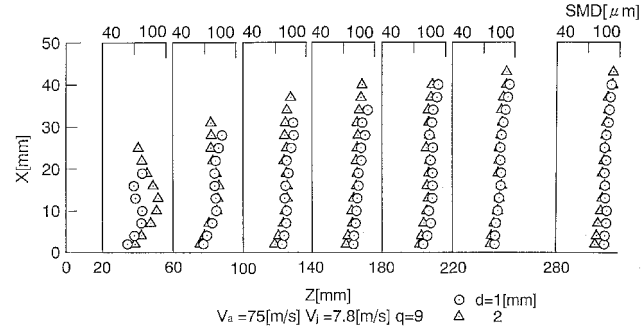

Fig. 10 Variations of mean droplet size distribution downstream at V_a = 75 m/s.

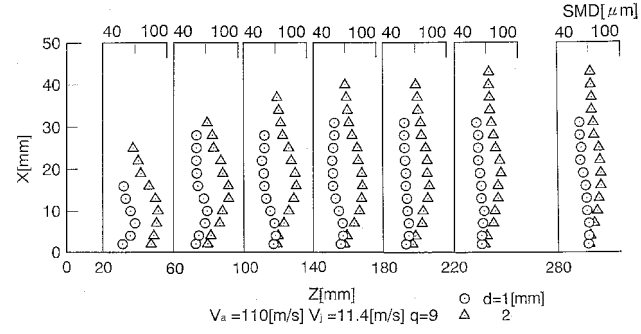

Fig. 11 Variations of mean droplet size distribution downstream at V_a = 110 m/s.

Figure 11 shows SMD variation at $V_a = 110$ m/s. For both conditions of $d = 1$ and 2 mm, SMD distributions have peaks in the core region throughout. SMDs of $d = 1$ mm are much smaller than those of $d = 2$ mm overall. The differences of SMD between $d = 1$ and 2 mm are appreciably large, even at $Z = 280$ mm.

Droplet Velocity

Figure 12 shows the variation of mean droplet velocity distribution for a 1-mm jet with momentum ratio at $Z = 180$ mm. Mean droplet velocity has a minimum value in the core region. It increases in the direction of liquid injection after it achieves a minimum value in the core region and then gradually decreases. This corresponds to the tendency of droplet size variation in the X direction as shown in Fig. 9. The mean droplet size decreases in the X direction after it reaches its maximum in the core region and it then increases toward the periphery. Thus, the periphery appears to consist of large droplets with low velocities that are generated by the disintegration of liquid clumps.

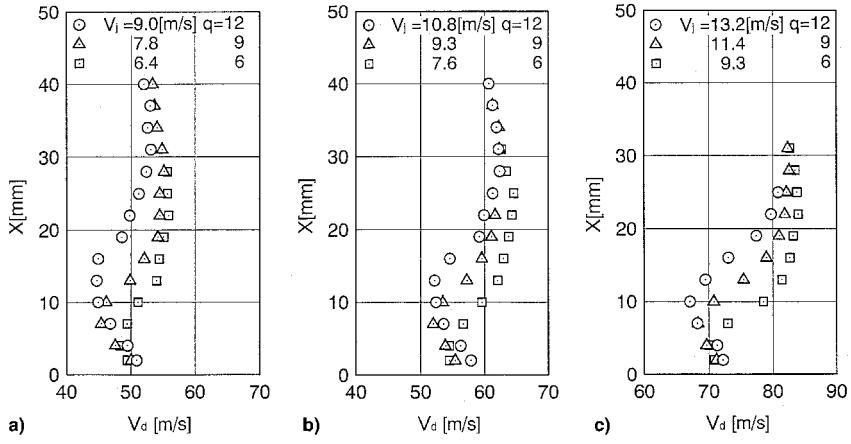

Fig. 12 Variations of mean droplet velocity distribution with momentum ratio. V_a = a) 75, b) 90, and c) 110 m/s.

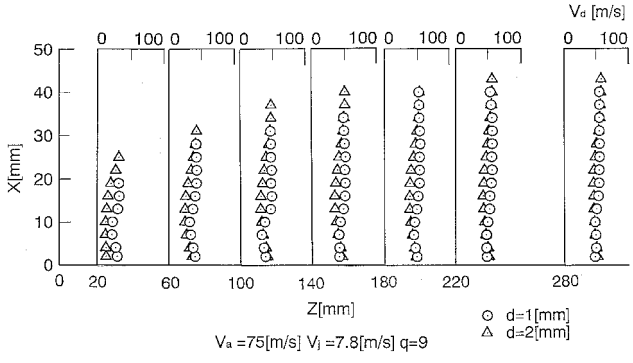

Fig. 13 Variations of mean droplet velocity distribution downstream at V_a = 75 m/s.

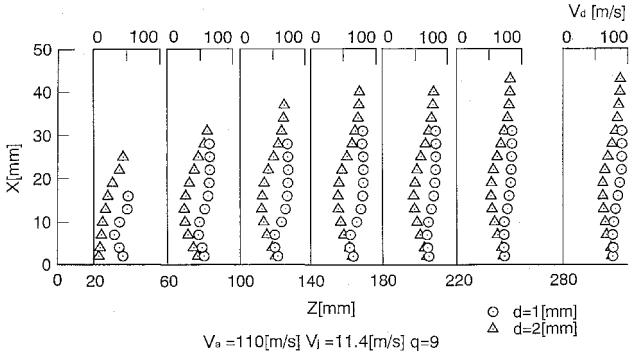

Fig. 14 Variations of mean droplet velocity distribution downstream at V_a = 110 m/s.

The droplet velocity totally increases with an increase in the air velocity. With an increase in the liquid-to-air momentum ratio, the minimum droplet velocity decreases and the vertical location where droplet velocity has a minimum value approaches the center from the bottom wall.

Figure 13 shows the variation in mean droplet velocity distribution in the Z direction at V_a = 75 m/s. In the vicinity of the liquid nozzle exit, the droplet velocity reaches its minimum in the core region and its maximum in the periphery. Mean droplet velocity distribution becomes uniform downstream. The influence of the liquid nozzle diameter on distribution is relatively small.

Figure 14 shows the mean droplet velocity distribution at V_a = 110 m/s. In the vicinity of the liquid nozzle exit, the droplet velocity distribution is similar to that at V_a = 75 m/s. However, it is nonuniform even at Z = 280 mm, in contrast with that of V_a = 75 m/s. The mean droplet velocities for the 2-mm jet are totally smaller than those for the 1-mm jet. The influence of the liquid nozzle diameter on the droplet velocity distribution is larger than that at V_a = 75 m/s. The tendency of the influence is stronger with regard to the liquid nozzle diameter on the droplet velocity, with an increase in air velocity the same as the tendency of the influence of the nozzle diameter regarding the average droplet size.

Conclusions

This study has been carried out to clarify the spray flow structure of a traversing liquid jet in a subsonic airstream. From photographic observation, surface waves on the liquid jet show not a two dimensional, but a more complicated structure, and they play important roles in the liquid jet disintegration process.

Droplet mass flux distribution in the X or Y direction can be presented by the standard normal function. The half-width of droplet mass flux distribution was obtained as a function of liquid-to-air momentum ratio and streamwise distance from the liquid nozzle. By means of the empirical equation of the droplet mass flux distribution in the X direction, the droplet dispersion is promoted in the upper region beyond the peak of the mass flux, and is lessened in the lower region with an increase in the liquid-to-air momentum ratio. With mass flux distribution in the Y direction, droplet dispersion is slightly promoted with an increase in the momentum ratio.

At low air velocity the droplet size reaches its maximum at the periphery of the jet plume. At high air velocity, however, it reaches its maximum in the core region. The maximum droplet size decreases downstream and the droplet size distribution approaches the uniform profile.

Droplet velocity reaches its minimum in the core region of the jet plume and the minimum droplet velocity decreases with an increase in the liquid-to-air momentum ratio. The minimum droplet velocity rapidly increases downstream. Thus, droplet velocity distribution approaches the uniform profile. Mean droplet velocities for the 2-mm jet are totally smaller than those for the 1-mm jet.

Acknowledgments

The authors express their thanks to N. Yatsuyanagi, A. Kumakawa, and H. Sakamoto for helpful discussions and comments, and to M. Tomita, K. Yoshimura, and M. Sei for their help with experiments.

References

[1]Baranovsky, S. I., and Schetz, J. A., "Effect of Injection Angle on Liquid Injection in Supersonic Flow," *AIAA Journal*, Vol. 18, No. 6, 1980, pp. 625–629.

[2]Schetz, J. A., Kush, E. A., Jr., and Joshi, P. B., "Wave Phenomena in Liquid Jet Breakup in a Supersonic Crossflow," *AIAA Journal*, Vol. 18, No. 7, 1980, pp. 774–778.

[3]Thomas, R. H., and Schetz, J. A., "Distributions Across the Plume of Transverse Liquid and Slurry Jets in Supersonic Airflow," *AIAA Journal*, Vol. 23, No. 12, 1985, pp. 1892–1901.

[4]Nejad, A. S., and Schetz, J. A., "Effects of Properties and Location in the Plume on Droplet Diameter for Injection in a Supersonic Stream," *AIAA Journal*, Vol. 21, No. 7, 1983, pp. 956–961.

[5]Less, D. M., and Schetz, J. A., "Penetration and Breakup of Slurry Jets in a Supersonic Stream," *AIAA Journal*, Vol. 21, No. 7, 1983, pp. 1045, 1046.

[6]Catton, I., Hill, D. E., and McRae, R. P., "Study of Liquid Jet Penetration in a Hypersonic Stream," *AIAA Journal*, Vol. 6, No. 11, 1968, pp. 2084–2089.

[7]Heister, S. D., Nguyen, T. T., and Karagozian, A. R., "Modeling of Liquid Jets Injected Transversely into a Supersonic Crossflow," *AIAA Journal*, Vol. 27, No. 12, 1989, pp. 1727–1734.

[8]Forde, J. M., Molder, S., and Szpiro, E. J., "Secondary Liquid Injection into a Supersonic Airstream," *Journal of Spacecraft and Rockets*, Vol. 3, No. 8, 1966, pp. 1172–1176.

[9]Schetz, J. A., and Padhye, A., "Penetration and Breakup of Liquids in Subsonic Airstreams," *AIAA Journal*, Vol. 15, No. 10, 1977, pp. 1385–1390.

[10]Kashiwagi, T., "Study on Afterburner of Aircraft Engine," *Ishikawajima-Harima Engineering Review*, Vol. 31, No. 2, 1991, pp. 109–114 (in Japanese).

[11]Oda, T., Hiroyasu, H., Arai, M., and Nishida, K., "Characteristics of Liquid Jet Atomization Across a High-Speed Airstream (1st Rep.)," *Transactions of the JSME*, Vol. 58, No. 552, 1992, pp. 2595–2606 (in Japanese).

[12]Inamura, T., Nagai, N., Watanabe, T., and Yatsuyanagi, N., "Disintegration of Liquid and Slurry Jets Traversing Subsonic Airstreams," *Proceedings of the 3rd World Conference on Experimental Heat Transfer, Fluid Mechanics and Thermodynamics* (Honolulu, HI), Elsevier, Amsterdam, 1993, pp. 1522–1529.

[13]Bowen, I. G., and Davies, G. P., Shell Research Ltd., Rept. ICT 28, London, 1951.

[14]Itoh, I., "Study of Spray Flow from Plain-Orifice Nozzle (3rd Rep.)," *Transactions of the JSME*, Vol. 36, No. 285, 1970, pp. 772–780 (in Japanese).

[15]Hetsroni, G., and Sokolov, M., "Distribution of Mass, Velocity, and Intensity of Turbulence in a Two-Phase Turbulent Jet," *Journal of Applied Mechanics*, Vol. 38, No. 6, 1971, pp. 315–327.

[16]Yatsuyanagi, N., "An Experimental and Analytical Study on Spray Flow Field by Liquid/Gas Coaxial Injector Elements(2)," Technical Rept. of National Aerospace Lab., TR-745, Dec. 1982 (in Japanese).

[17]Inamura, T., Nagai, N., Hirai, T., and Asano, H., "Disintegration Phenomena of Metalized Slurry Fuel Jets in High Speed Air Stream," *Proceedings of the 5th International Conference on Liquid Atomization and Spray Systems*, National Inst. of Standards and Technology, Gaithersburg, MD, 1991, pp. 839–846.